Supporting Information for

Two-dimensional self-assembled structures of highly ordered bioactive crystalline-based block copolymers

Sylvia Ganda[§], Martin Dulle[†], Markus Drechsler[ǂ], Beate Förster[ǂ], Stephan Förster[†,*] and Martina H. Stenzel[§,*]

[§]Centre for Advanced Macromolecular Design, School of Chemistry, The University of New South Wales, UNSW, Sydney, NSW 2052, Australia

[ǂ]Bavarian Polymer Institute (BPI), Keylab for Electron and Optical Microscopy, [†]Physikalische Chemie I, University of Bayreuth, D-95447 Bayreuth, Germany

*To whom correspondence should be addressed, e-mail: M.Stenzel@unsw.edu.au, stephan.foerster@uni-bayreuth.de

General Experimental Considerations

Chemicals. 1-*O*-A*i*PrFru and BMDO monomers were synthesized as described previously[1]. 1-*O*-A*i*PrFru monomer was purified by column chromatography. BMDO, ε-CL and MCL monomers were purified by distillation under reduced pressure and polymerizations carried out under inert atmosphere. All BCPs were prepared via reversible addition-fragmentation chain-transfer (RAFT) polymerization as reported previously. Sample **6** $PMCL_{121}$-*b*-PF_{81} was synthesized by following the similar procedure as to PCL block copolymers where PCL macro-RAFT agent was replaced with PMCL macro-RAFT agent. Polymer characterization of the BCPs are provided in Table S1. D-Fructose, *o*-benzene dimethanol, bromodimethyl acetaldehyde and ε-caprolactone were purchased from Sigma-Aldrich and used as received unless stated otherwise. Anhydrous toluene was obtained from PureSolv MD 7 solvent purification system (Innovative Technology, Inc., Galway, Ireland) packed with activated alumina columns to remove water and trace impurities. The water sensitivity of BMDO monomer and ring-opening polymerization of ε-CL and MCL requires that the polymerization procedures to be performed under an inert and dry atmosphere through the use of glovebox and Schlenk line techniques.

Methods

Nuclear magnetic resonance (NMR) spectroscopy was performed using either a Bruker Avance III 300, 5 mm BBFO probe (300.17 MHz, ^{1}H: 300.17 MHz, ^{13}C: 75.48) or an Avance III 400, 5 mm BBFO probe (400.13 MHz, ^{1}H: 400.13 MHz, ^{13}C: 100.62). NMR spectra were processed using Bruker TOPSPIN 3.2 software. Samples were analyzed in either $CDCl_3$ or DMSO-d6 as stated accordingly. All chemical shifts are stated in parts per million ppm (δ) relative to tetramethylsilane (δ = 0 ppm), referenced to the chemical shifts of residual solvent resonances

(^{1}H and ^{13}C). Data is reported as follows: chemical shift [multiplicity (s = singlet, d = doublet, dd = doublet of doublets, t = triplet, m = multiplet), integration is reported as multiples of protons, proton identity, *J* (denotes the coupling constants and is measured in Hertz)].

Size exclusion chromatography (SEC) was carried out using a Shimandzu modular system containing a DGU-12A degasser, a LC-10AT pump, a SIL-10AD automatic injector, a CTO-10A column oven, and a RID-10A differential refractive index detector. A PL 5.0 micrometre bead-size guard column (50 x 7.5 mm^2) followed by four 300 × 7.8 mm linear PL (Styragel) columns (10^5, 10^4, 10^3 and 500 Å pore size) were used for the analyses. *N*,*N*-dimethylacetamide [DMAC, HPLC grade; 0.03% w/v LiBr, 0.05% 2,6-dibutyl-4-methylphenol (BHT)] with a flow rate of 1 mL.min^{-1} was used as the mobile phase with an injection volume of 50 µL at 50°C. The unit calibration was conducted over commercially available narrow molecular weight distribution polystyrene standards (0.5 – 1,000 kDa, Polymer Laboratories). Chromatograms were processed using Cirrus 2.0 software (Polymer Laboratories).

Dynamic light scattering (DLS) measurements employed a Malvern Zetasier Nano ZS instrument equipped with a 4 mV He – Ne laser operating at λ = 632 nm and non-invasive backscatter detection at 173°. Measurements were carried out in a disposable cuvette at 25°C, provided 15 equilibration period prior to each set of measurements. For a given sample, a total of three measurements were conducted with the number of runs, attenuator and path length being automatically adjusted by the instrument, depending on the sample quality.

Transmission electron microscopy (TEM). The micrographs were obtained in bright-field mode from a JEOL 1400 TEM with the electron beam voltage operating at 100 kV equipped with a Gatan CCD for the acquisition of the digital micrographs. The TEM sample grids were prepared by drop-casting 5.0 µL of the nanoparticle solution onto Formvar-coated copper grid and left to settle for 3 min before blotting with filter paper. The contrast of the nanoparticles was enhanced by negative staining with uranyl acetate for 5 min followed by water washing.

Transmission electron microscopy-selected-area electron diffraction (TEM-SAED). The micrographs were obtained in bright-field mode from a Zeiss LEO 922 Omega EFTEM (Zeiss Microscopy GmbH, Jena, Germany) with the electron beam voltage operating at 200 kV equipped with a Gatan CCD for the acquisition of the digital micrographs. The TEM sample grids were prepared by drop-casting 2.0 µL of the nanoparticle solution onto a hydrophilized carbon-coated copper grid and left to settle for 1 min before blotting with filter paper. Selected-area electron diffraction (SAED) experiments were carried out on the same microscope. Staining was not used in these experiments to avoid secondary diffraction pattern except for PMCL-*b*-PF where phosphotungstic acid (PTA) was used to stain the grid for 1 min. This was necessary to increase the contrast due to the small size of the micelles and low electron density of the sample.

Cryo-Transmission Electron Microscopy (Cryo-TEM). A sample droplet of 2.0 µL was put on a lacey carbon filmed copper grid (Science Services, Muenchen), which was hydrophilized by air

plasma glow discharge (30 s with 50 W, Solarus 950, Gatan, Muenchen, Germany). Subsequently, most of the liquid was removed with blotting paper leaving a thin film stretched over the lace holes. The specimens were instantly shock frozen by rapid immersion into liquid ethane cooled to approximately 90 K by liquid nitrogen in a temperature-controlled freezing unit (Zeiss Cryobox, Carl Zeiss Microscopy GmbH, Jena, Germany). The temperature was monitored and kept constant in the chamber during all the sample preparation steps. The specimen was inserted into a cryotransfer holder (CT3500, Gatan, Muenchen, Germany) and transferred to a Zeiss / LEO EM922 Omega EFTEM (Zeiss Microscopy GmbH, Jena, Germany). Examinations were carried out at temperatures around 90 K. The TEM was operated at an acceleration voltage of 200kV. Zero-loss filtered images ($\mathbf{\Delta}$E = 0 eV) were taken under reduced dose conditions (100 – 1000 e/nm^2). All images were registered digitally by a bottom mounted CCD camera system (Ultrascan 1000, Gatan, Muenchen, Germany) combined and processed with a digital imaging processing system (Digital Micrograph GMS 1.9, Gatan, Muenchen, Germany).

The dimensions of platelet micelles and area, width and length distribution were determined by using the software program ImageJ from the National Institutes of Health. At least 200 micelles were measured by the software and computed for statistical analyses to obtain the area, width and length information. The number-average length (L_n), weight-average length (L_w), number-average width (W_n), weight-average width (W_w), number-average area (A_n) and weight-average area (A_w) of the platelets were calculated using the equations below (L, W are the length and width of object respectively; N, number and A, area of object).

$$L_n = \frac{\sum_{i=1}^{n} N_i L_i}{\sum_{i=1}^{n} N_i} \qquad L_w = \frac{\sum_{i=1}^{n} N_i L_i^2}{\sum_{i=1}^{n} N_i L_i} \qquad W_n = \frac{\sum_{i=1}^{n} N_i W_i}{\sum_{i=1}^{n} N_i} \qquad W_w = \frac{\sum_{i=1}^{n} N_i W_i^2}{\sum_{i=1}^{n} N_i W_i}$$

$$A_n = \frac{\sum_{i=1}^{n} N_i A_i}{\sum_{i=1}^{n} N_i} \qquad A_w = \frac{\sum_{i=1}^{n} N_i A_i^2}{\sum_{i=1}^{n} N_i A_i}$$

Cryo-Scanning Electron Microscopy (Cryo-SEM). Cryo-scanning electron microscopy (cryo-SEM) was carried out at a Zeiss Ultraplus field emission scanning electron microscope (FESEM) equipped with a Leica cryo unit. Platelet micelle aqueous solution was vitrified by plunge-freezing in liquid nitrogen. The frozen samples were freeze-fractured in a Leica MED 020, etched for 60 s at 10^{-6} mbar at -105°C. The samples were imaged with an in-lens detector at a voltage of 1.0 kV.

Synthesis

Synthesis of 6-methyl-ε-caprolactone (MCL). This synthesis followed a literature procedure with slight modifications[2]. 10.0 g of 2-methyl-cyclohexanone (0.0891 mol, 1 equiv.) was dissolved in 550 mL of methanol:H_2O mixture (1:1 v/v %) containing excess sodium bicarbonate (0.490 mol, 5.5 equiv.) to mitigate the acidity of reaction mixture. The solution was stirred at room temperature for a few minutes until completely dissolved. Oxone (0.178 mol, 2 equiv.) was added into the solution in two portions under vigorous stirring. The reaction was allowed to react under stirring at room temperature for 6 h. Following, the insoluble salts were removed by filtration and methanol removed under reduced pressure. The product was then extracted with dichloromethane for 3 times and dried over magnesium sulfate. The salt was filtered away and the solvent removed under reduced pressure yielding MCL in the form of yellow liquid. The monomer was characterized by using ^{1}H NMR spectroscopy to yield 97% of 6-methyl-ε-caprolactone and 3% of 2-methyl-ε-caprolactone (2-MCL). The monomer was further purified by distillation under reduced pressure to remove water and traces of impurities before ring-opening polymerization took place.

Polymer Characterization

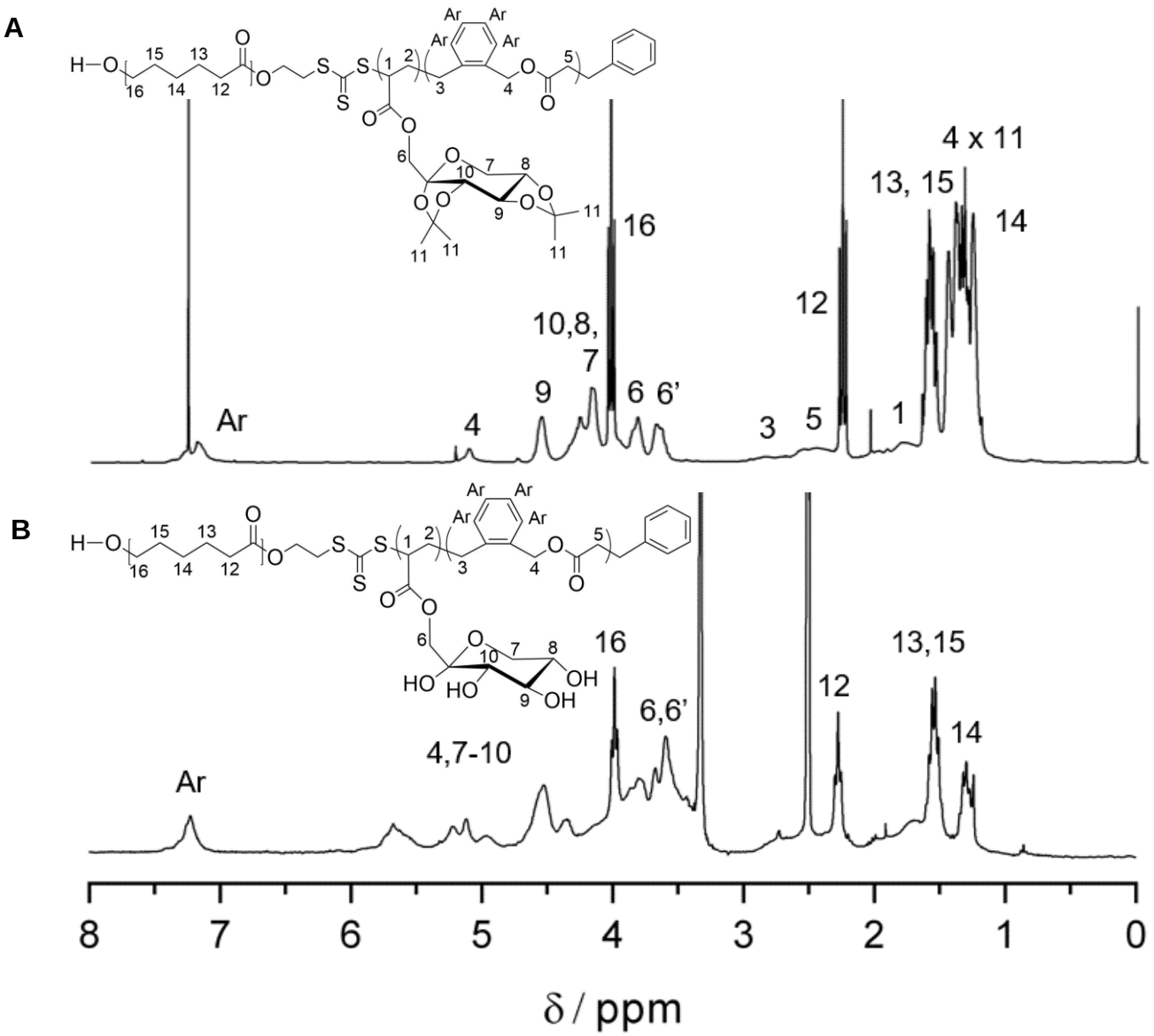

Figure S1. ^{1}H NMR spectra (300.17 MHz) of (a) PCL-*b*-P(*i*PrF-*co*-BMDO) (in $CDCl_3$) and (b) PCL-*b*-P(F-*co*-BMDO) (in DMSO-d6) after deprotection of the sugar moieties showing complete disappearance of the isopropylidene protecting groups. The presence of PCL peaks after deprotection suggests that the removal of protecting groups did not cleave off the PCL block.

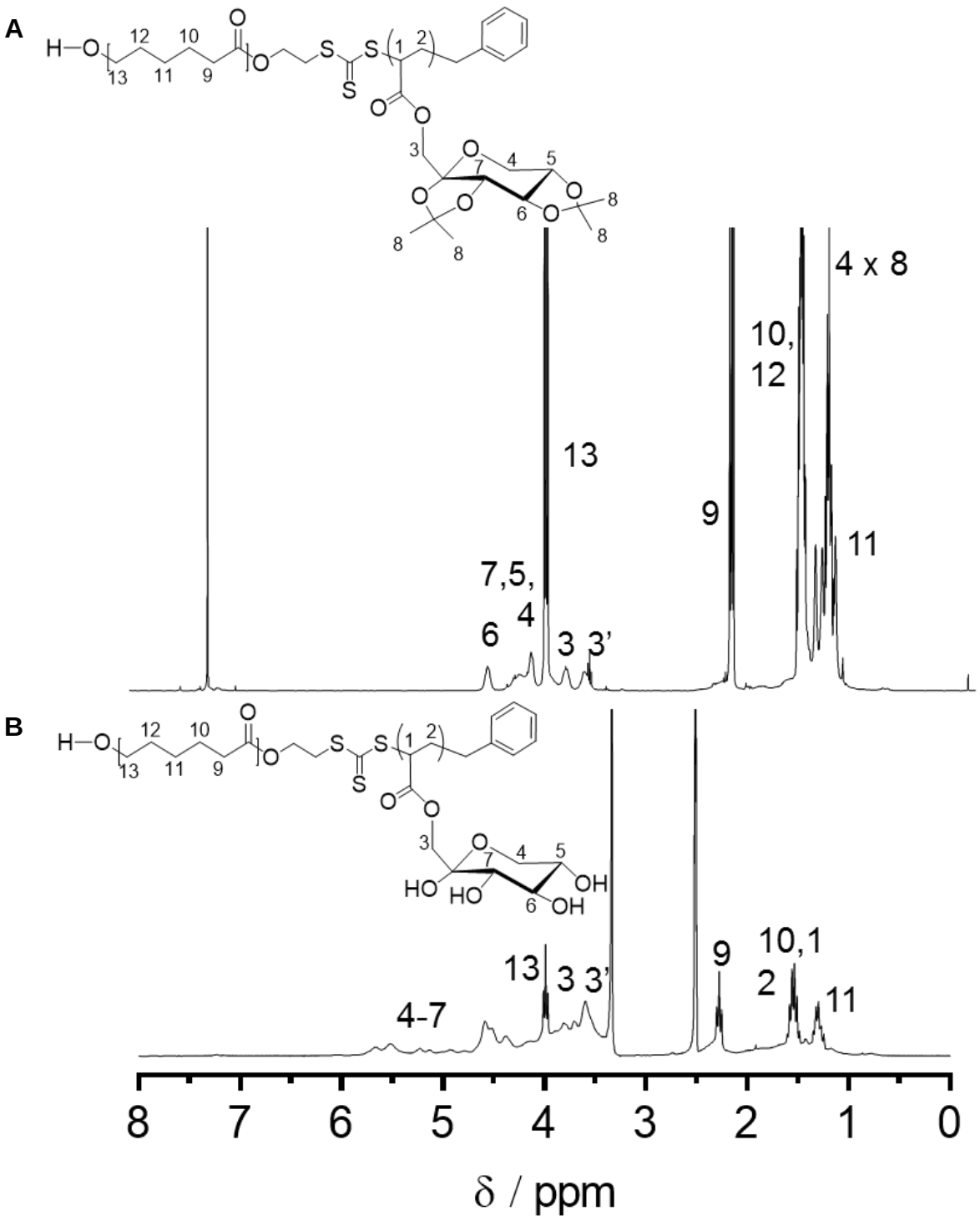

Figure S2. ^{1}H NMR spectra (400.17 MHz) of (a) PCL-*b*-P(*i*PrF) (in $CDCl_3$) and (b) PCL-*b*-PF (in DMSO-d6) after deprotection of the sugar moieties showing complete disappearance of the isopropylidene protecting groups. The presence of PCL peaks after deprotection suggests that the removal of protecting groups did not cleave off the PCL block.

Preparation of platelet micelles. The self-assembly of block copolymers was performed upon deprotection of the carbohydrate moieties by removing the isopropylidene protecting groups under acidic condition. Following, 4.0 mg of the corresponding block copolymer solid was dissolved in 2.0 mL of dimethylsulfoxide (DMSO) as the selective solvent for both blocks. The polymer was heated up to 90°C to allow for complete dissolution and allowed to cool to room temperature. 2.0 mL of milliQ H_2O was then added slowly to the polymer solution at the controlled rate of 0.20 $mL \cdot h^{-1}$to reach the final concentration of 1.0 $mg \cdot mL^{-1}$. The solution was dialyzed against water for 2 days to remove the organic solvent.

Seeded growth of platelet micelles *via* living crystallization-driven self-assembly (CDSA) of PCL_{101}-*b*-PF_{178} (3). The seeded-growth of PCL platelet solution with or without dialysis beforehand yields different morphologies with distinguished pathways. Herein, the pre-formed PCL platelet micelles were used as the seed precursors to the seeded growth of the crystalline structure. 0.010 mL of BCP **3** PCL_{101}-*b*-PF_{178} unimers as a 10 $mg \cdot mL^{-1}$ DMSO solution was added to 0.100 mL of PCL_{101}-*b*-PF_{178} platelet solution at the concentration of 0.67 $mg \cdot mL^{-1}$ (with dialysis) and 1.0 $mg \cdot mL^{-1}$ (without dialysis) respectively. Upon addition of the unimers, the solution was mixed briskly by shaking for 5 s using a vortex agitator. The solutions were then allowed to age at room temperature and in the fridge (3 – 4°C) for 2 months and aliquots were drawn at different time points.

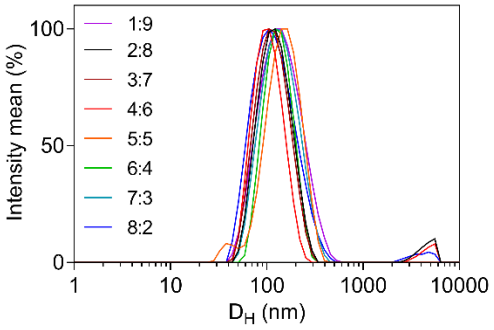

Figure S3. Dynamic light scattering (DLS) measurements of the BCP PCL_{101}-*b*-PF_{78} (1.0 $mg \cdot mL^{-1}$) dissolved in different amount of DMSO followed by the addition of H_2O – expressed in DMSO:H_2O (v/v %) solvent mixtures.

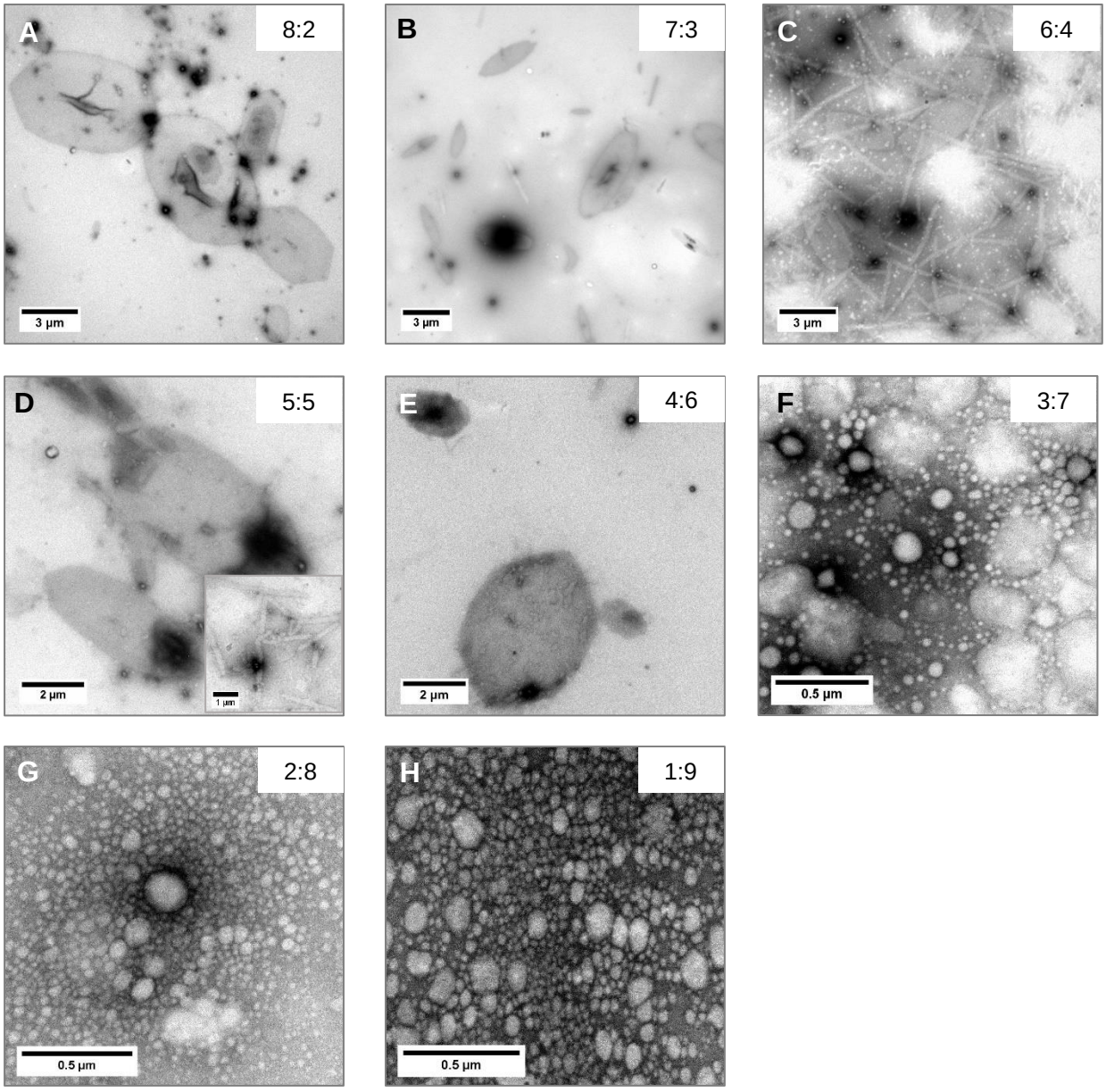

Figure S4. The effects of solvent quality towards the structure formation of BCP **1** PCL_{101}-*b*-PF_{78} with platelet size reduction towards the formation of spherical micelles with the increasing non-solvent (water) ratio in the order of (**A**) to (**H**) (8:2 – 1:9 DMSO:H_2O v/v % co-solvent mixtures), as indicated by TEM. Only spherical micelles and irregular large-compound micelles were observed instead of 2D platelets starting from 70% water content.

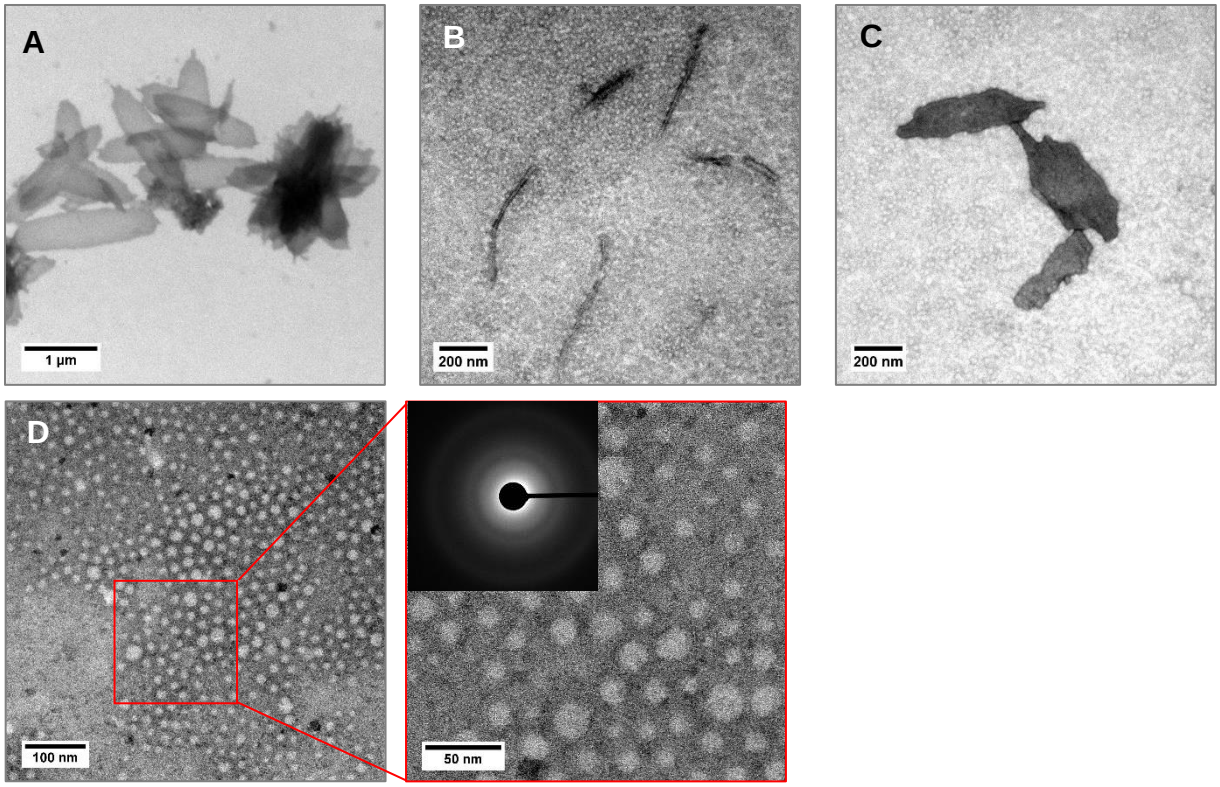

Figure S5. TEM micrographs of (**A – C**) PCL_{101}-*b*-PF_{88} block copolymers self-assembly forming platelet micelles with the presence of spherical micelles and ill-defined structures; and (**D**) $PMCL_{121}$-*b*-PF_{88} spherical micelles prepared at room temperature. The inset in (**D**) denotes an area where electron diffraction experiment (TEM-SAED) was carried out indicating the absence of crystalline diffraction pattern. This sample was negatively stained with phosphotungstic acid (PTA) to enhance the contrast.

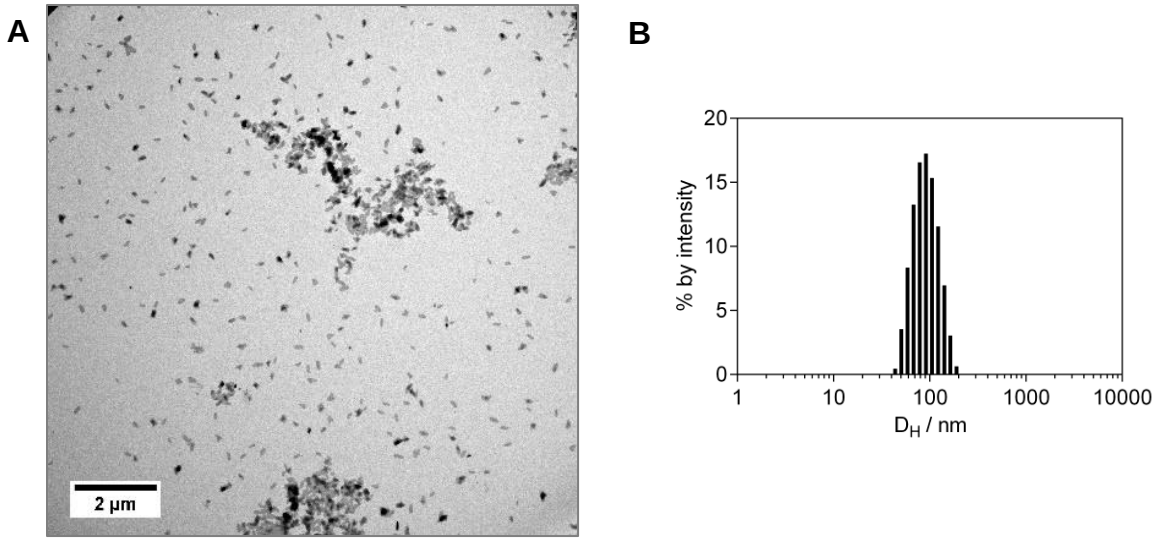

Figure S6. (**A**) TEM micrograph and (**B**) DLS histogram of BCP **4** PCL_{106}-*b*-P[F_{69}-*co*-$BMDO_9$] nanoplatelets formed by the slow addition of water in DMSO containing BCP solution followed by dialysis (1.0 mg·mL^{-1}, water addition rate at 0.2 mL·h^{-1}). DLS revealed the hydrodynamic diameter (D_H) of the nanoplatelets to be 106 nm (PDI = 0.085, intensity mean).

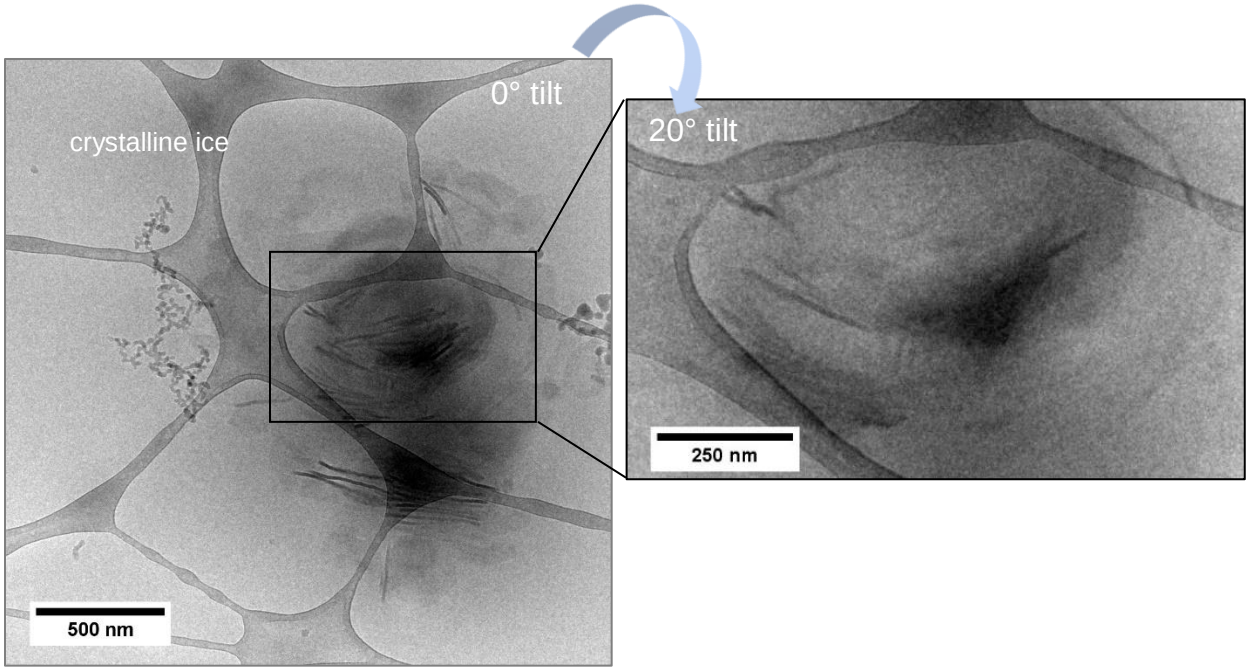

Figure S7. Nanoplatelets prepared by the self-assembly of BCP **4** PCL_{106}-*b*-P[F_{69}-*co*-$BMDO_9$] (in DMSO) by the slow addition of water (5:5 v/v %, 1.0 $mg \cdot mL^{-1}$) upon removal of organic phase, micrographs recorded at 20°C tilt angle. Notice the edge-on orientation of the nanoplatelets depicting the overall thickness of structure (10.5 nm). The disappearance of the high gray value (dark regions) thin disk-like structures denoted the change in structural geometry upon tilting indicating non- rod-like structures.

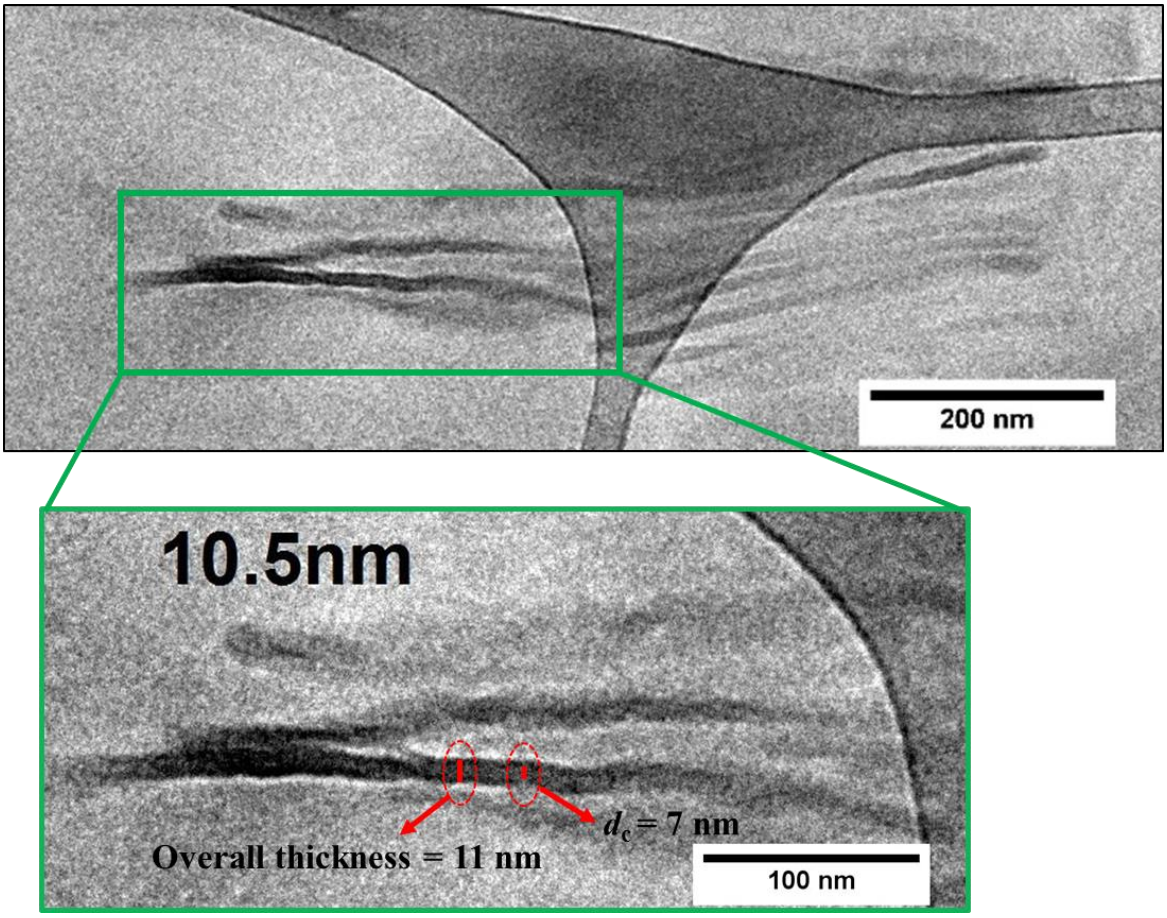

Figure S8. Cryo-TEM micrograph showing several nanoplatelets of BCP **4** PCL_{106}-*b*-P(F_{69}-*co*-$BMDO_9$) along the edge view with face to face configuration. The overall thickness is measured by taking the cross-sectional height of the platelets as indicated by the double-headed arrow in the inset. Meanwhile, the core diameter (d_c) of these platelets was deduced and estimated by taking the grey value across the overall thickness of the platelets. As can be seen in the inset, the core is the lighter region sandwiched between two darker regions (lower grey value), which suggests that these are the carbohydrate corona with a higher electron density, giving higher contrast. Therefore, the lighter region within the particle is the core. However, it is important to note that a clear disparate solvent-swollen corona structure was unable to be obtained independently.

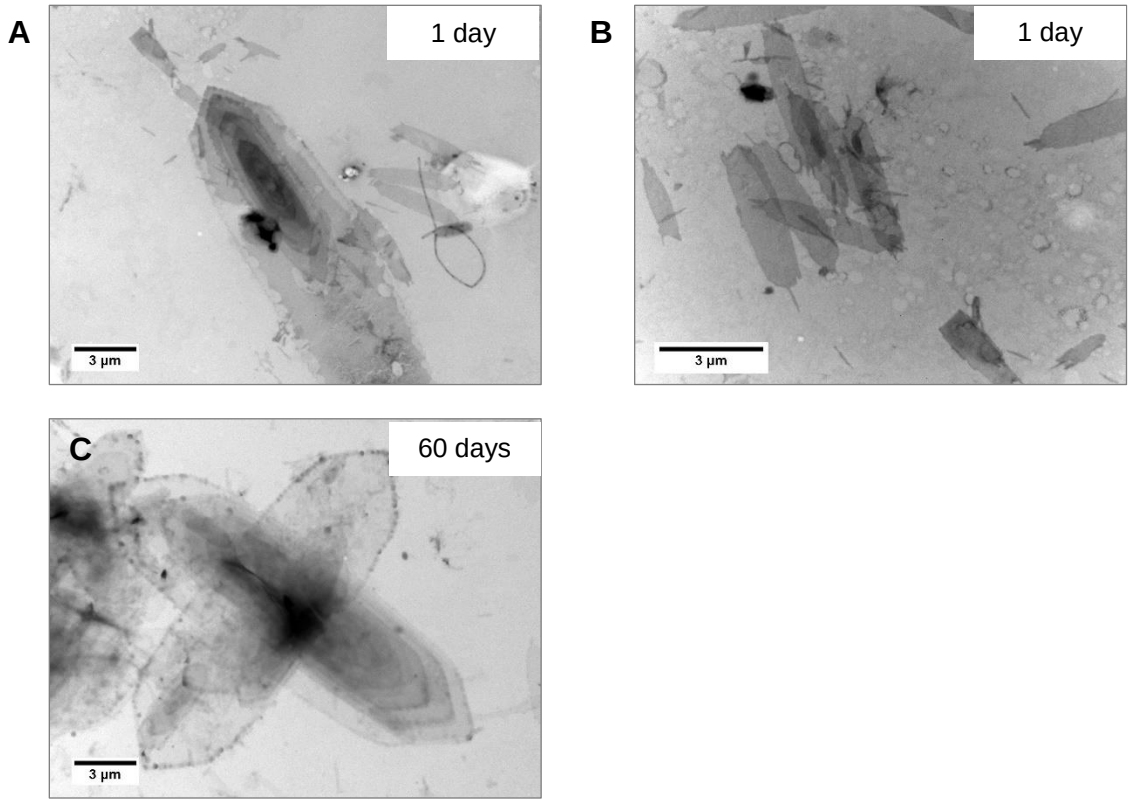

Figure S9. Time dependent morphological evolution of living crystallization-driven self-assembly of BCP **3** PCL_{101}-*b*-PF_{178} by adding PCL_{101}-*b*-PF_{178} unimers (10.0 µL, 10.0 mg·mL^{-1}) to the seed 2D platelet solution aged at 3 – 4°C at different periods: (**A – B**) 1 day and (**C**) 60 days.

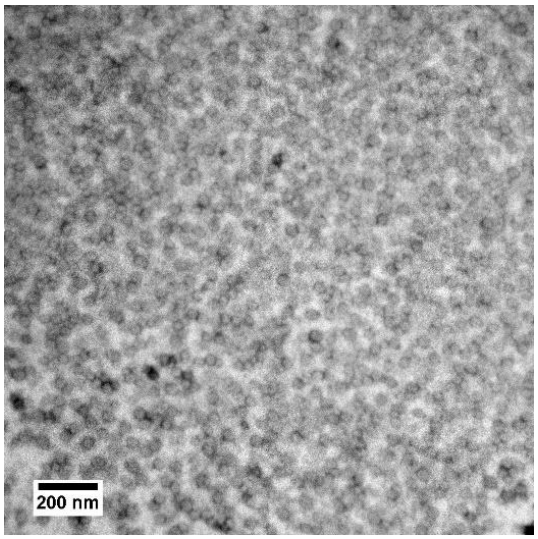

Figure S10. The presence of metastable spherical micelles (ca. 20 – 40 nm) as the first stage of crystallization-driven self-assembly of BCP **3** PCL_{101}-*b*-PF_{178}. When a precipitant for the PCL block was introduced, phase separation led to the formation of these aggregates. Due to the slow kinetics of this process to reach thermodynamic equilibrium, the morphological evolution by fusion of these micelles to 2D lamellae structures driven by crystallization force was observed.

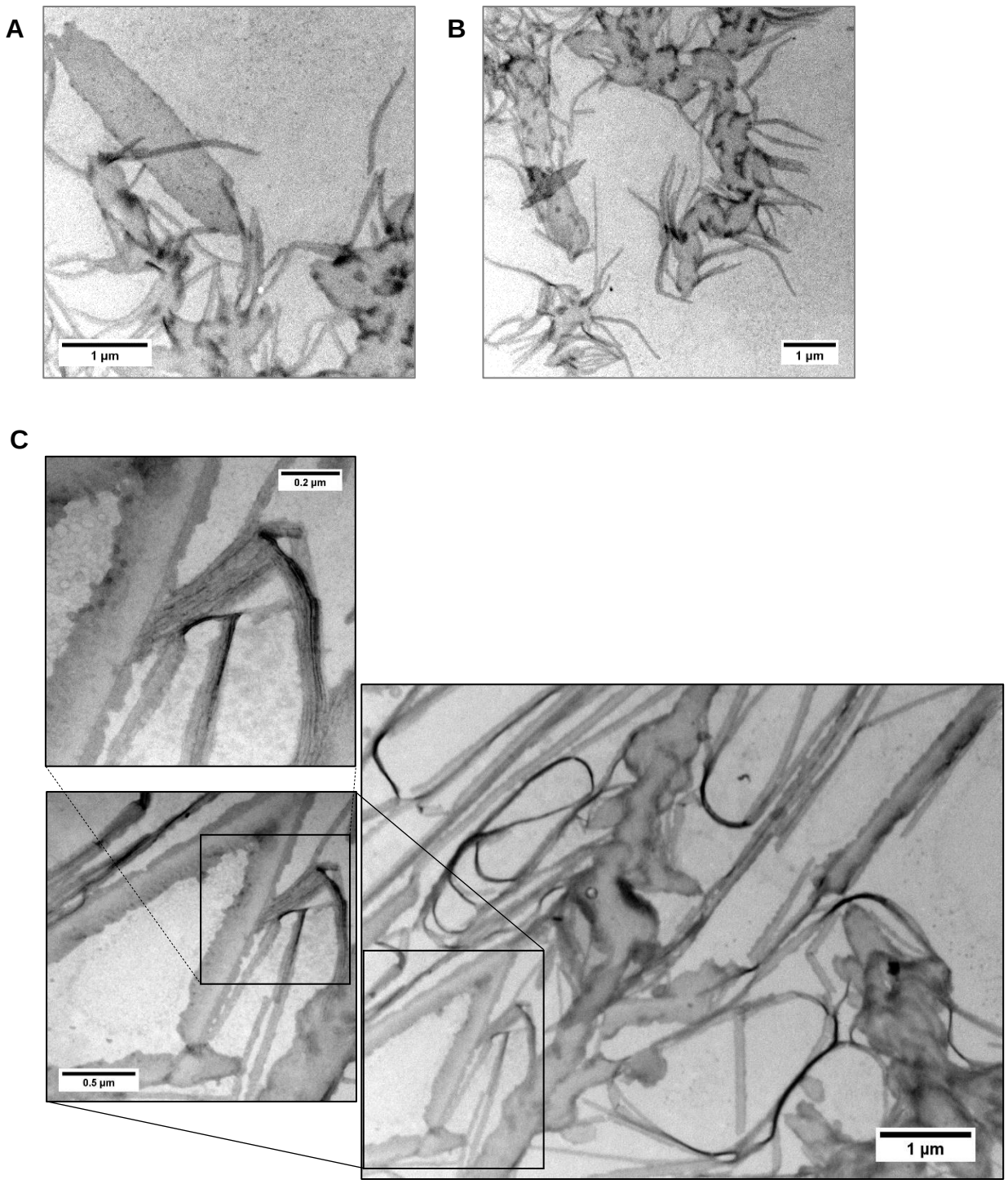

Figure S11. TEM micrographs of a drop-cast aliquot of the seeded growth of BCP **3** platelet micelle solution immediately after unimers addition showing intermediate structures. We observed the co-existence of (**A**) rods, platelets, (**B – C**) tubes, sheets, and ribbons.

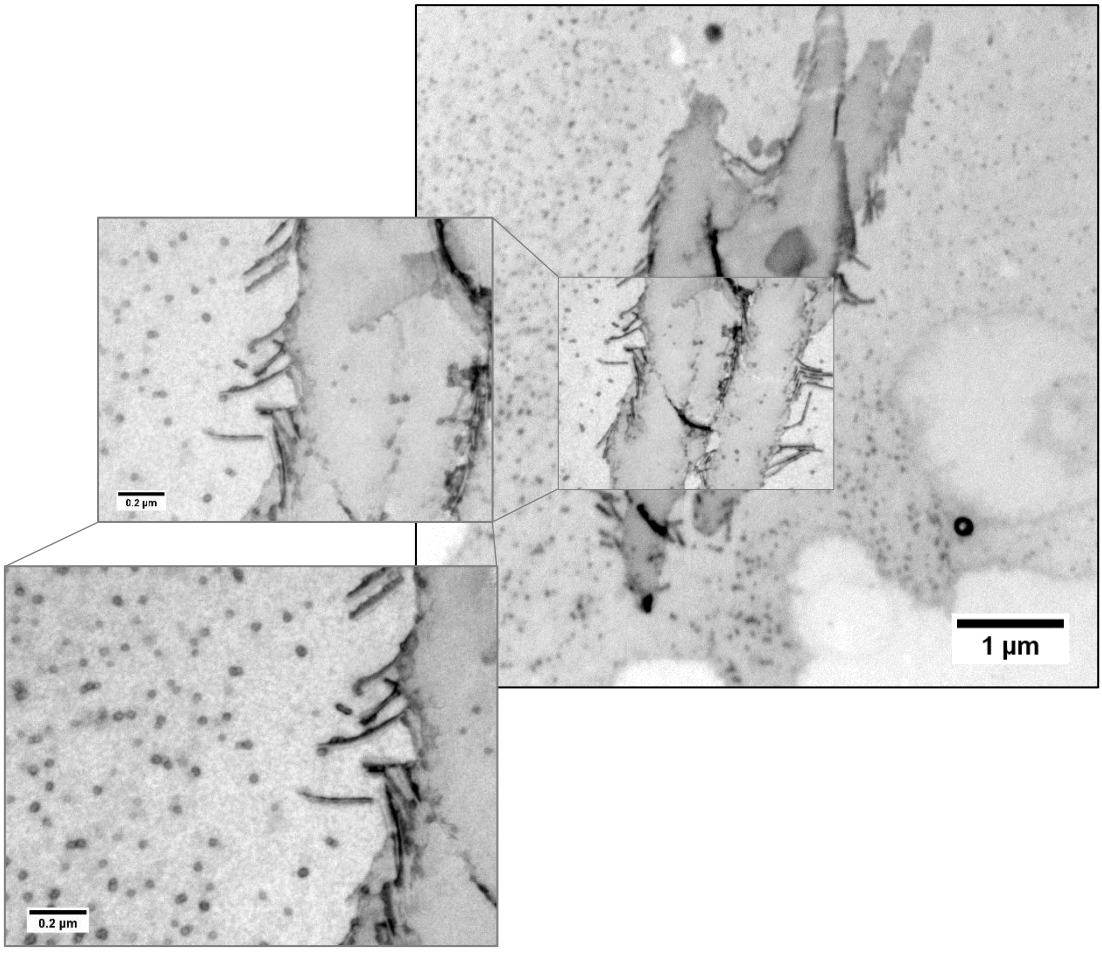

Figure S12. TEM micrographs of a drop-cast aliquot of the seeded growth of BCP **3** platelet micelle solution immediately after unimers addition showing intermediate structures. The insets display the morphological transformation pathway through fusion of spherical micelles to rods and lamella sheets for non-dialyzed sample. The displayed micrograph consists two separate TEM images because the dimensions of the sheets were too great for the magnification used to resolve the nanostructure.

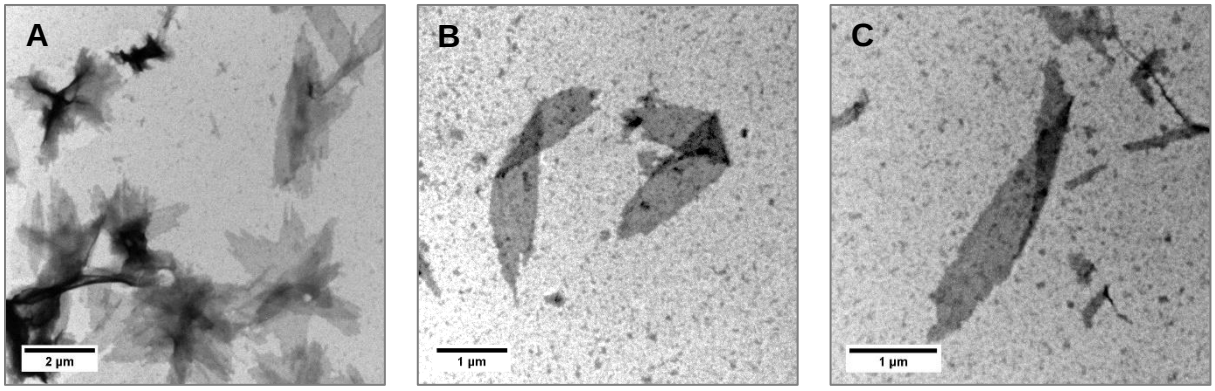

Figure S13. TEM micrographs of a drop-cast aliquot of the seeded growth of BCP **3** platelet micelle solution after 30 days of ageing of PCL_{101}-b-PF_{178} at room temperature. The intermediate structures were no longer observed in this sample.

REFERENCES

1. Ganda, S.; Jiang, Y.; Thomas, D. S.; Eliezar, J.; Stenzel, M. H., Biodegradable Glycopolymeric Micelles Obtained by RAFT-controlled Radical Ring-Opening Polymerization. *Macromolecules* **2016,** *49* (11), 4136-4146.

2. Martello, M. T.; Hillmyer, M. A., Polylactide–poly (6-methyl-ε-caprolactone)–polylactide thermoplastic elastomers. *Macromolecules* **2011,** *44* (21), 8537-8545.